

## Ni<sub>50</sub>Mn<sub>36</sub>Sn<sub>14</sub> Heusler Alaşımının Yumuşak Manyetik Karakteri

Ayşe DURAN\*<sup>1</sup>

<sup>1</sup>Dumlupınar Üniversitesi, Kütahya Teknik Bilimler MYO, Elektronik ve Otomasyon Bölümü,  
Kütahya

Geliş tarihi: 03.11.2017

Kabul tarihi: 29.06.2018

### Öz

Bu çalışmada, Mn<sub>2</sub> ve Sn<sub>1</sub> bileşenleri antiferromanyetik etkileşimli Ni<sub>50</sub>Mn<sub>36</sub>Sn<sub>14</sub> Heusler alaşımının (NiMnSn-HA) manyetik özellikleri, etkin alan teorisinde Kaneyoshi yaklaşımı kullanılarak araştırılmıştır. NiMnSn-HA ve bileşenleri, T<sub>C</sub>'de ikinci derece faz geçişi, Mn<sub>2</sub> bileşeni ayrıca T<sub>i</sub>'de zayıf bir birinci derece faz geçişi and dalgalı bir histerezis davranışı sergiler. T<sub>i</sub>'nin altında, NiMnSn-HA ve bileşenleri, yüksek zorlayıcılığa bağlı sert bir manyetik karakteristik gösterirken sıcaklık T<sub>C</sub>'ye yaklaştıkça yumuşak manyetikler. Bu davranışların, Mn<sub>2</sub> ve Sn<sub>1</sub> bileşenlerinin antiferromanyetik etkileşiminden kaynaklandığı söylenebilir.

**Anahtar Kelimeler:** Ni<sub>50</sub>Mn<sub>36</sub>Sn<sub>14</sub> Heusler alaşımı, Yumuşak manyetik karakter, Histeris eğrileri, Zorlayıcılık, Etkin alan teorisi

### Soft Magnetic Characteristic of Ni<sub>50</sub>Mn<sub>36</sub>Sn<sub>14</sub> Heusler Alloy

#### Abstract

In this study, the magnetic properties of Ni<sub>50</sub>Mn<sub>36</sub>Sn<sub>14</sub> Heusler alloy (NiMnSn-HA) with the antiferromagnetic interaction between Mn<sub>2</sub> and Sn<sub>1</sub> components were investigated by using Kaneyoshi approach within the effective field theory. NiMnSn-HA and its components display the second order phase transition. Its Mn<sub>2</sub> component also exhibit a weak first order at T<sub>i</sub> and a fluctuating hysteresis behavior below T<sub>i</sub>. While NiMnSn-HA and its components show a hard magnetic characteristic below T<sub>i</sub>. They are soft magnetic as the temperature approaches to T<sub>C</sub>. It can be said that these behaviors are due to antiferromagnetic interaction between Mn<sub>2</sub> and Sn<sub>1</sub> components.

**Keywords:** Ni<sub>50</sub>Mn<sub>36</sub>Sn<sub>14</sub> Heusler alloy, Soft magnetic characteristic, Hysteresis loops, Coercivity, Effective field theory

---

\*Sorumlu yazar (Corresponding author): Ayşe DURAN, [ayse.duran@dpu.edu.tr](mailto:ayse.duran@dpu.edu.tr)

## 1. INTRODUCTION

Materials called soft magnetic have low coercivity; on the other hand those named hard magnetic possess high coercivity [1]. There are a variety of soft magnetic alloys being commercially important: ferrites, iron and low-carbon steels, iron-silicon, iron-aluminum-silicon, nickel-iron, iron-cobalt, and amorphous alloys. Detecting the soft magnetic characteristic of the material is still of great interest as it is important to many commercial areas: T.V. shadow mask, T.V. gun, lead frame, induction cooking, magnetic shielding, sensor, etc. It was experimentally reported by Wei et al. Fe-Co-Ni-Si-B high entropy amorphous alloys composites (HEAACs) show good soft magnetic properties [2]. The synthesised and characterised elastomer materials with a complex hybrid filler based on large magnetically hard grains of FeNdB and small magnetically soft carbonyl iron particles and investigations on magnetic hybrid Elastomers (MHEs) for their technical implementation as sensor systems with adaptive magnetically controllable sensitivity range made by Becker et al. [3]. Fan et al. investigated the silane surface modification effect on the microstructure, temperature resistance, tensile strength, rated current under DC-bias superposition and magnetic properties of phosphatized iron-based soft magnetic composites (SMCs) playing a key role in power chip inductors, making operating at higher rated currents possible [4]. Alnasir et al. studied the magnetic properties of nanoparticles of Gd<sub>5</sub>Si<sub>4</sub> and its substitutional derivatives to explore their efficacy of as agents of self-controlled magnetic hyperthermia [5]. Hsiang et al searched for the effect on the relationships between the phosphate insulation coating microstructure and physical and magnetic properties of iron-based soft magnetic composites [6]. Sunday et al examined the future of SMCs, which required low core losses and high magnetic permeability at various frequency ranges for diverse applications such as aerospace and automobiles [7]. Lauda et al carried on studying the magnetic properties of a new soft magnetic composite consisting of a commercial FeSi

powder, whose particles are covered with MnZn ferrite as an insulating layer [8]. A novel magnetic hysteresis behavior in BaTi<sub>1.2</sub>Co<sub>1.2</sub>Fe<sub>9</sub>O<sub>19.8</sub> ferrite at low temperature was investigated by Feng et al. [9]. Magnetic performance of the MnNi-FeCo core-shell nanostructures tuned by the thickness and stoichiometry of the FeCo Shell was studied by Shen et al. [10] and the electrodeposition of NiMn nanowires in AAO template performed in chloride bath and the crystal structure, morphology, and the magnetic properties of nanowires by Fathi et al. [11]. There are theoretical investigations on the composition-dependent crystal structure, elastic modulus, phase stability, and magnetic property of Ni<sub>2-x</sub>Co<sub>x</sub>Mn<sub>1.60</sub>Sn<sub>0.40</sub> studied by using first-principles calculations in combination with atomistic spin dynamics method by Li et al. [12]. The example of  $\alpha$ -Fe crystal by using Quantum model of a hysteresis in a single-domain magnetically soft ferromagnetic was searched for by Ignatiev et al. [13]. The hysteresis phenomena for small NiMnGa single crystals embedded in a polymer matrix for slowly varying magnetic fields were reported by Conti et al. [14] and the hysteresis behaviours of a Ising-type-segmented nanowire on the dependence of the composition, temperature and geometric by Kantar [15].

The magnetic properties of NiMnSn Heusler alloys were investigated experimentally and theoretically. There are experimentally investigations on the formation of the Ni<sub>2</sub>MnSn Heusler alloy by solid state reaction from elemental powders [16]. The effects of boron addition on the microstructure, magnetic, mechanical, and shape memory properties of Ni<sub>50</sub>Mn<sub>40-x</sub>Sn<sub>10</sub>B<sub>x</sub> polycrystalline alloys were examined [17]. The effects of the composition alteration on the magnetization and shape memory behavior of Ni<sub>50</sub>Mn<sub>40-x</sub>Sn<sub>10+x</sub> alloys were reported [18]. The microstructural and phase transition characteristics of melt spun ribbons of Heusler alloys with starting selected compositions Ni<sub>50</sub>Mn<sub>37</sub>Sn<sub>13</sub>, Ni<sub>50</sub>Mn<sub>36</sub>Sn<sub>14</sub>, and Ni<sub>50</sub>Mn<sub>40</sub>Sn<sub>10</sub> were given in the literature [19]. The crystal structure and morphological and crystallographic features of the microstructure in 40 modulated

martensite of an NiMnSn alloy were given [20]. Temperature dependent magnetostrains in polycrystalline magnetic shape memory Heusler alloys were mentioned [21]. The cytotoxicity and ion release from an Ni<sub>50</sub>Mn<sub>36</sub>Sn<sub>14</sub> atomic percent composition meta-magnetic shape memory alloy were evaluated using NIH/3T3 fibroblasts [22]. The magnetic properties of the parent and martensite phases of Ni<sub>2</sub>Mn<sub>1+x</sub>Sn<sub>1-x</sub> and Ni<sub>2</sub>Mn<sub>1+x</sub>In<sub>1-x</sub> and the magnetic field-induced shape memory effect obtained in NiCoMnIn alloy were reported [23]. The martensitic transition and magnetic entropy change of the Ni<sub>51</sub>Mn<sub>49-x</sub>Sn<sub>x</sub> were searched for [24]. Magnetic and magneto-optical properties NiMnSb<sub>1-x</sub>Sn<sub>x</sub> compounds [25] and the giant magnetic refrigeration capacity of Co-doped in a Ni<sub>40</sub>Co<sub>10</sub>Mn<sub>40</sub>Sn<sub>10</sub> HA were mentioned [26]. The effect of Fe substitution on the antiferromagnetic fraction in martensitic Ni<sub>2</sub>Mn<sub>1.44</sub>Sn<sub>0.56</sub>-type HA [27], and the magnetic characterizations of the intermartensitic phase transition in Ni<sub>50</sub>Mn<sub>38</sub>Sn<sub>12</sub> HA ribbons were given [28]. The effect of Si doping at Sn site on structural, magnetic and exchange bias properties of the HA system Ni<sub>50</sub>Mn<sub>36</sub>Sn<sub>14-x</sub>Si<sub>x</sub> were studied [29]. Nevertheless, there are rare investigations with using first-principles calculations, Monte Carlo calculation and effective field theory (EFT) on the NiMnSn Heusler alloys can be seen in the literature on the magnetic properties of the metamagnetic Heusler alloy (Ni, Co)-Mn-Sn by means of first principles simulations [30], the phase transitions in Ni-Mn(Z)-Sn (Z=3d transition metals) [31], and the influence of the valance electron concentration on the tetragonal transformation in Ni<sub>2</sub>Mn<sub>1+x</sub>Sn<sub>1-x</sub> and Co<sub>2</sub>Ni<sub>1+x</sub>Ga<sub>1-x</sub> [32], and the martensitic phase transition and phase stability of Ni<sub>8</sub>Mn<sub>6</sub>Sn<sub>2-x</sub>In<sub>x</sub> shape memory alloys were studied [33]. The magnetic and structural properties of Ni(Cu, Co)MnSn Heusler alloys for the magnetocaloric effect were investigated by using density functional theory combined with Monte Carlo simulations of a classical Heisenberg model [34], lattice location effect of Ni<sub>50</sub>Mn<sub>36</sub>Sn<sub>14</sub> HA and surface superconductivity in Ni<sub>50</sub>Mn<sub>36</sub>Sn<sub>14</sub> HA were examined by using Kaneyoshi approach within effective field theory (EFT) [35, 36]. In this

work, the magnetic properties of Ni<sub>50</sub>Mn<sub>36</sub>Sn<sub>14</sub> HA are investigated by using Kaneyoshi approach (KA) [37-40] within the effective field theory. There are many researches by using Kaneyoshi approach within EFT: the binary Nickel/Bismuth alloy [41], the honeycomb structured thin film [42], single-, two- and three-layer [43-45], Ising nanographene systems, and carbon diamond nanolattice [46], composite Ising nanoparticles consisting of core and shell [47], cubic nanowire [48], the sc, bcc and fcc nanolattices [49], hexagonal Ising nanowire [50], the nanowire system consisting of composite core and shell [51], transverse Ising nanowire [52], cubic nanowire with core and shell [53], cylindrical Ising nanowires [54-55], the cylindrical core and shell spin-1 ising nanowire [56], spin-1 Ising nanotube [57], the kinetic cylindrical Ising nanotube [58], cylindrical transverse spin-1 Ising nanowire [59], Ising-type segmented nanowire (ISN) [15], the antiferromagnetic YBCO-7 superconductor [60], one-dimensional Ising system (1DIS) [61], a Ising-type endohedral fullerene (EF) with a doped magnetic spin-1/2 particle confined within a spherical cage (by diluted magnetic spin-1 particles) [62], etc.

In the present study, it is aimed to obtain hard and soft magnetic characteristics of Ni<sub>50</sub>Mn<sub>36</sub>Sn<sub>14</sub> Heusler Alloy with antiferromagnetic exchange interaction between Mn2 and Sn1. It is assumed that Ni<sub>50</sub>Mn<sub>36</sub>Sn<sub>14</sub> Heusler Alloy consists of spin-1/2 Ising particles [35,36]. Its magnetic properties is investigated by using Kaneyoshi approach (KA) within the effective field theory.

The paper is arranged as follows. In Section 2, the theoretical method is given. The detailed numerical results and discussions are presented in Section 3. Finally, Section 4 is devoted to a summary and a brief conclusion.

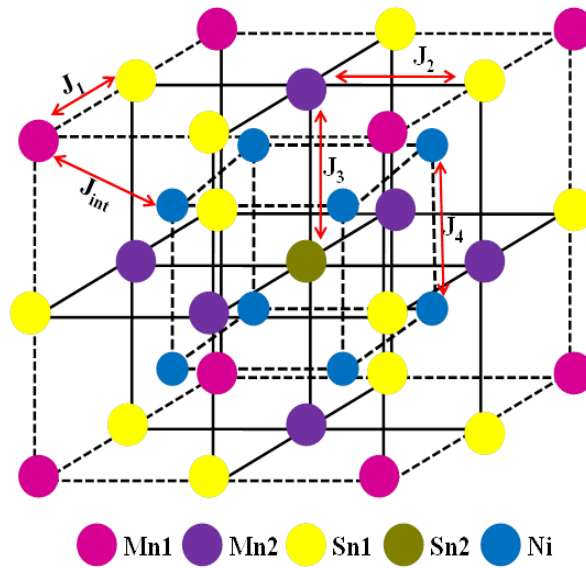
## 2. THEORETICAL METHOD

In our previous works, it was investigated that the lattice location effect of Ni<sub>50</sub>Mn<sub>36</sub>Sn<sub>14</sub> HA, where

all the exchange interactions are ferromagnetic ( $J_1, J_2, J_3, J_4$  and  $J_{int} > 0$ ) [35], and the surface superconductivity in Ni<sub>50</sub>Mn<sub>36</sub>Sn<sub>14</sub> HA, where exchange interaction between Ni and Mn or Sn components is antiferromagnetic and the other exchange interactions are ferromagnetic ( $J_1, J_2, J_3, J_4 > 0$  and  $J_{int} < 0$ ) [36]. In this work, the effect of the antiferromagnetic exchange interaction between Mn2 and Sn1 components ( $J_1, J_3, J_4$  and  $J_{int} > 0$  and

$J_2 < 0$ ) on the magnetic properties of Ni<sub>50</sub>Mn<sub>36</sub>Sn<sub>14</sub> Heusler alloy were studied by using Kaneyoshi approach within EFT. The schematic representation of NiMnSn-HA and its components is presented in Fig. 1 [35,36]. It is assumed that NiMnSn-HA has five different magnetic atoms and they are Mn1, Mn2, Sn1, Sn2 and Ni, which are spin-1/2 particles [35,36].

Unit cell of Ni<sub>50</sub>Mn<sub>36</sub>Sn<sub>14</sub> Heusler Alloy with L<sub>21</sub> structure



$J_1$ : Mn1-Sn1  $J_2$ : Mn2-Sn1  $J_3$ : Mn2-Sn2  $J_4$ : Ni-Ni  $J_{int}$ : Ni-Mn or Sn

**Figure 1.** The modeled crystal structure of NiMnSn-HA and its components [35,36]

$$\begin{aligned}
 H = & -J_1 \sum_{\langle \text{Mn1,Sn1} \rangle} S_{\text{Mn1}}^z S_{\text{Sn1}}^z - J_2 \sum_{\langle \text{Sn1,Mn2} \rangle} S_{\text{Sn1}}^z S_{\text{Mn2}}^z - J_3 \sum_{\langle \text{Mn2,Sn2} \rangle} S_{\text{Mn2}}^z S_{\text{Sn2}}^z - J_4 \sum_{\langle \text{Ni,Ni} \rangle} S_{\text{Ni}}^z S_{\text{Ni}}^z \\
 & - J_{int} \sum_{\langle \text{Ni,Mn or Sn} \rangle} S_{\text{Ni}}^z S_{\text{Mn or Sn}}^z - h \left( \sum_{\text{Mn1}} S_{\text{Mn1}}^z + \sum_{\text{Mn2}} S_{\text{Mn2}}^z + \sum_{\text{Sn1}} S_{\text{Sn1}}^z + \sum_{\text{Sn2}} S_{\text{Sn2}}^z + \sum_{\text{Ni}} S_{\text{Ni}}^z \right)
 \end{aligned}
 \tag{1}$$

The Ising Hamiltonian of NiMnSn-HA is given by, where,  $S^z = \pm 1$  is the Pauli spin operator.  $h$  is the external magnetic field.  $J_1$  (between Mn1 and Sn1),  $J_2$  (between Mn2 and Sn1),  $J_3$  (between Mn2 and Sn2),  $J_4$  (between Ni atoms) and  $J_{int}$  (between Mn1 or Mn2 or Sn1 or Sn2 and Ni atoms) are the exchange interactions between two nearest-

neighbor atoms of the lattice of NiMnSn-HA. The interactions are obtained by using the relation that  $J = k/nd$  [35, 36, 41, 43, 46, 49], where,  $nd$  is the normalized lattice constant that obtained from the real lattice constant ( $d = 5.9931 \text{ \AA}$ ) of NiMnSn-HA [29,35,36] and defined as  $nd = d/1 \text{ \AA}$ .  $J_1, J_2, J_3, J_4$  and  $J_{int}$  are given by as follows:

$J_1=J_3=J_4=2k/nd=0.3337$ ,  $k=1>0$  (ferromagnetic)  
 $J_2=2k/nd=-0.3337$ ,  $k=-1<0$  (antiferromagnetic)  
 $J_{int}=4k/(\sqrt{3}nd)=0.3854$ ,  $k=1>0$  (ferromagnetic)

The magnetizations of NiMnSn-HA and its components by using Kaneyoshi approach [35, 36] are given by

$$\begin{aligned} Ac &= \cosh(J_1 \nabla), As = \sinh(J_1 \nabla) \\ Bc &= \cosh(J_2 \nabla), Bs = \sinh(J_2 \nabla) \\ Cc &= \cosh(J_3 \nabla), Cs = \sinh(J_3 \nabla) \\ Dc &= \cosh(J_4 \nabla), Ds = \sinh(J_4 \nabla) \\ Ec &= \cosh(J_{int} \nabla), Es = \sinh(J_{int} \nabla) \end{aligned} \quad (2)$$

$$\begin{aligned} m_{Mn1} &= \left[ Ac + m_{Sn1} As \right]^3 \left[ Ec + m_{Ni} Es \right]^1 F_{s-1/2}(x) \Big|_{x=0}, \\ m_{Mn2} &= \left[ Bc + m_{Sn1} Bs \right]^4 \left[ Cc + m_{Sn2} Cs \right]^1 \left[ Ec + m_{Ni} Es \right]^4 F_{s-1/2}(x) \Big|_{x=0}, \\ m_{Sn1} &= \left[ Ac + m_{Mn1} As \right]^2 \left[ Bc + m_{Mn2} Bs \right]^2 \left[ Ec + m_{Ni} Es \right]^2 F_{s-1/2}(x) \Big|_{x=0}, \\ m_{Sn2} &= \left[ Cc + m_{Mn2} Cs \right]^6 \left[ Ec + m_{Ni} Es \right]^8 F_{s-1/2}(x) \Big|_{x=0}, \\ m_{Ni} &= \left[ Dc + m_{Ni} Ds \right]^3 \left[ Ec + m_{Mn1} Es \right]^1 \left[ Ec + m_{Mn2} Es \right]^3 \left[ Ec + m_{Sn1} Es \right]^3 \left[ Ec + m_{Sn2} Es \right]^1 F_{s-1/2}(x) \Big|_{x=0}, \\ m_{Ni_{50}Mn_{36}Sn_{14}} &= \frac{1}{35} \left[ 8m_{Mn1} + 6m_{Mn2} + 12m_{Sn1} + m_{Sn2} + 8m_{Ni} \right] \end{aligned} \quad (3)$$

where,  $\nabla = \partial/\partial x$  is the differential operator and the function of  $F_{s-1/2}(x)$  is defined by as follows for the spin-1/2 Ising particles.

$$F_{s-1/2}(x) = \tanh[\beta(x+h)] \quad (4)$$

$$\beta = 1/(k_B T_A) \quad (5)$$

where,  $k_B$  and  $T_A$  is the Boltzmann's constant and the absolute temperature, respectively. In this work, the temperature and the external magnetic field is  $T = k_B T_A / J$  and  $H=h/J$ , respectively.  $T_A$  is an absolute temperature, and its unit is Kelvin.  $T$  is a reduced temperature, and it has no any unit. Furthermore,  $H$  is a reduced external magnetic field. Namely,  $J$  (Joule) $=k_B T_A$ ;  $T_A = J$  (Joule) $/k_B$  (Kelvin);  $T=k_B T_A/J$  (Joule) $=$ Kelvin/Kelvin $=$ unitless. It is used that “ $T$ ” (the reduced temperature) instead of “ $k_B T_A/J$ ” and “ $H$ ” (the

reduced external magnetic field) instead of “ $h/J$ ” in all of the figures and in our paper.

### 3. THE NUMERICAL RESULTS

It is depicted that the magnetization versus temperature plots of NiMnSn-HA and its components (Mn1, Mn2, Sn1, Sn2, and Ni) at zero external magnetic field ( $M(T)$  plots) as seen in Fig. 2. The HA and its components, except for its Mn2 components, display the only one second-order phase transitions from the ferromagnetic (F) phase to paramagnetic (P) phase at  $T_C=2.204$  (where  $T_C$  is Curie Temperature). This ferromagnetic behavior of the HA is a quantitatively in accordance with the theoretical report of  $Ni_{50}Mn_{36}Sn_{14}$  Heusler alloy by Duran [35] and with the experimental reports of the  $Mn^{57}Fe$ -y  $Ni_2Mn_{1.44}Sn_{0.56}$  sample by Passamani et al. [27].

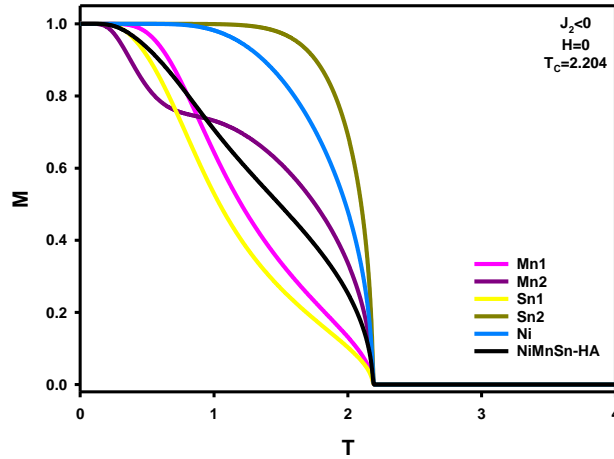


**Figure 2.** The crystal structure of NiMnSn-HA and its components

The Mn2 component display a reentrant phase transition not only the weak first order phase transition, which it appears like a second order phase transition at the transition point, from F to F at transformation temperature ( $T_1$ ) both also the second phase transition from F to P at  $T_C$ . It is known that first-order phase transitions display a wide variety of behaviors and thermodynamic quantities generally show the discontinuity behavior or s-shape at the transition temperatures. Furthermore, the first-order phase transitions which appear like a second-order at the transition point are named as weak first order phase transitions [63-65]. It is clearly seen that the reentrant behavior of the Mn2 component is due to antiferromagnetic interaction between Mn2 and Sn1 components. It is thought that the reentrant behavior of the Mn2 component is due to antiferromagnetic interaction between Mn2 and Sn1 components. This reentrant phase transition is in good agreement with the reentrant phase transition of simple cubic spin-1 Ising model at low temperature region reported by Özkan et al. [63].

In Fig. 3a-f, the magnetization versus the external magnetic field curves of NiMnSn-HA and its components ( $M(H)$  curves) were presented to investigate the effect of the temperature on the hysteresis loops at  $T < T_1$ . It was clearly seen that NiMnSn-HA and its components have the hysteresis loops with hard ferromagnetic

characteristic, which is related to high coercivity. These results, except for those of its Mn2 components, are a quantitatively good accordance with the theoretical report of Ni<sub>50</sub>Mn<sub>36</sub>Sn<sub>14</sub> Heusler alloy by Duran [35] and with the experimental reports of Ni<sub>50</sub>Mn<sub>36</sub>Sn<sub>14</sub> alloy by Li et al. [66], Mn<sub>2</sub>Ni<sub>1.6</sub>Sn<sub>0.4</sub> melt-spun ribbons by Singh et al. [67], Ni<sub>50</sub>Mn<sub>36</sub>Sn<sub>14-x</sub>Si<sub>x</sub> alloys by Raji et al. [29], Ni<sub>50</sub>Mn<sub>40-x</sub>Sn<sub>10+x</sub> alloys by Aydogdu et al. [18]. In Fig. 3a-f, the magnetic hysteresis loops of NiMnSn-HA and its components have the same decreasing coercive field ( $H_C$ ) while the temperature increases from 0.25 to 0.55, but they have the same increasing coercive field while the temperature is at  $0.55 < T < 1.00$ . They have the same  $H_C$  started to decrease at  $T=1.00$ .

As the temperature increase, while the remanence magnetizations ( $M_r$ ) values of its Sn2 and Ni components equal to 1 in Fig. 3d and Fig. 3e, the  $M_r$  values of NiMnSn-HA and other components decrease as seen in Fig. 3a-c and 3f. On the other hands, its Sn2 and Ni components display a sharp F hysteresis loop at  $T < T_1$ . It is said that its Sn2 and Ni components can have harder ferromagnetic characteristic because of the higher coercive fields according to those of NiMnSn-HA and other components at  $T < T_1$ . In addition, in Fig. 3b, its Mn2 component displays a fluctuating ferromagnetic hysteresis behavior unlike the others.

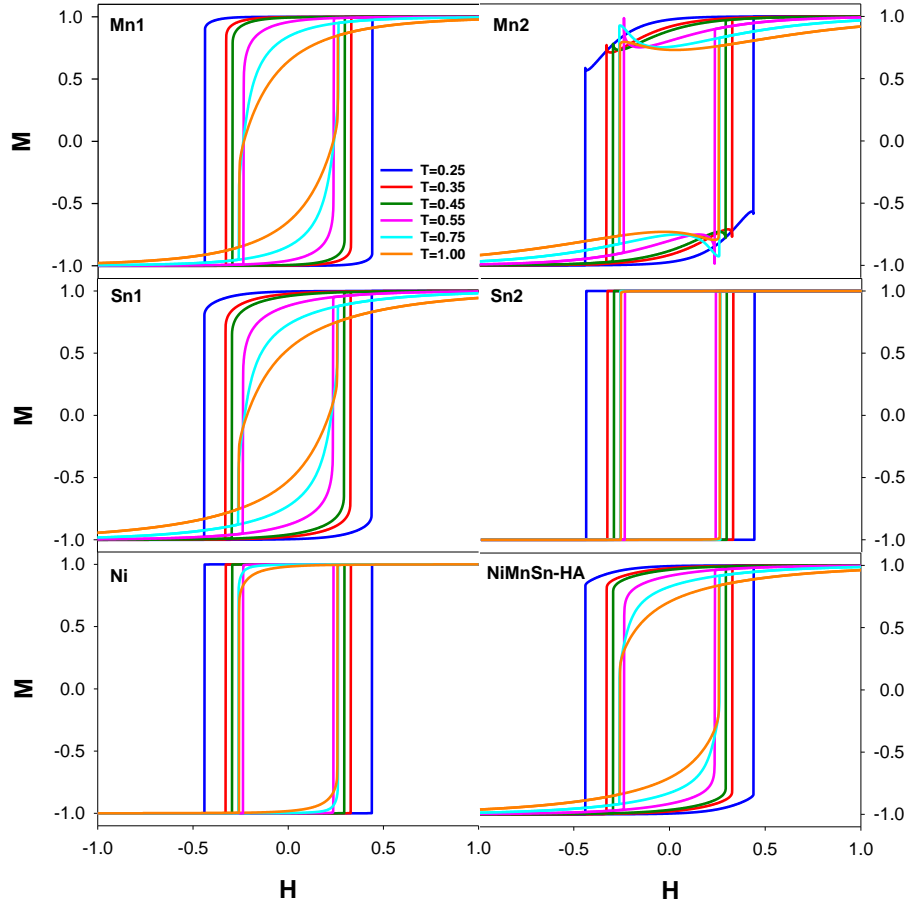


**Figure 3.**  $M(H)$  magnetic hysteresis loops of, (a) Mn1, (b) Mn2, (c) Sn1, (d) Sn2, (e) Ni component and (f) NiMnSn-HA for  $T < T_c$

It is thought that the fluctuating ferromagnetic hysteresis behavior of the Mn2 component is due to antiferromagnetic interaction between Mn2 and Sn1 components. At  $T=0.25$ , it starts to decrease at  $H=0.432$  while the magnetization increase from  $-1.000$  to  $-0.678$  between  $-1.000 \leq H \leq 0.431$ . This behavior continues to the magnetization value of  $-0.586$  at  $H=0.439$  and the magnetization rises suddenly up  $1.000$  at  $H_c=0.440$ . At  $T=0.35$ , similarly, it starts to decrease at  $H=0.307$  while the magnetization increases from  $-1.000$  to  $-0.711$  between  $-1.000 \leq H \leq 0.306$ . This behavior continues to the magnetization value of  $-0.770$  at  $H=0.328$  and the magnetization rises suddenly up  $0.986$  at  $H_c=0.329$ . At  $T=0.45$ , similarly, it starts to decrease at  $H=0.264$  while the magnetization

increases from  $-1.000$  to  $-0.731$  between  $-1.000 \leq H \leq 0.263$ . This behavior continues to the magnetization value of  $-0.780$  at  $H=0.294$  and the magnetization rises suddenly up  $0.970$  at  $H_c=0.295$ . At  $T=0.55$ , similarly, it starts to decrease at  $H=0.154$  while the magnetization increases from  $-1.000$  to  $-0.752$  between  $-1.000 \leq H \leq 0.153$ . This behavior continues to the magnetization value of  $-0.987$  at  $H=0.237$  and the magnetization rises suddenly up  $0.898$  at  $H_c=0.238$ . At  $T=0.75$ , while the magnetization increases from  $-0.969$  to  $-0.752$  between  $-1.000 \leq H \leq 0.045$ . it decreases up to  $-0.928$  at  $0.046 \leq H \leq 0.258$  and it starts to increase at  $H=0.259$ . This behavior continues to the magnetization value of  $-0.922$  at  $H=0.261$  and the

magnetization rises suddenly up 0.828 at  $H=0.262$ . For  $T=1.00$ , while the magnetization decreases from -0.919 to -0.749 between  $-1.000 \leq H \leq 0.236$  it starts to increase at  $H=0.237$ . This behavior continues to the magnetization value of -0.748 at  $H=0.258$  and the magnetization rises suddenly up 0.762 at  $H_C=0.259$ .

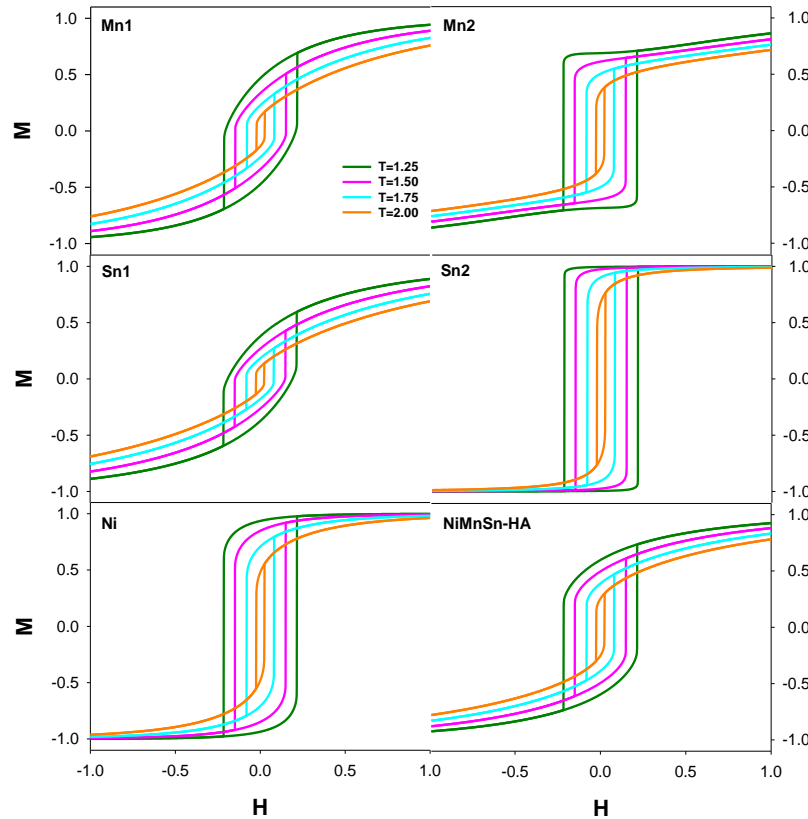


**Figure 4.**  $M(H)$  magnetic hysteresis loops of (a) Mn1, (b) Mn2, (c) Sn1, (d) Sn2, (e) Ni component and (f) NiMnSn-HA for  $T_1 < T < T_C$

In Fig. 4a-f,  $M(H)$  curves of  $Ni_{50}Mn_{36}Sn_{14}$  Heusler alloy and its components for  $T_1 < T < T_C$  are depicted. It can clearly be seen that NiMnSn-HA and its components have the F hysteresis loops. The hysteresis loops of  $Ni_{50}Mn_{36}Sn_{14}$  and its component have the same coercive field ( $H_C$ ) decreasing as the temperature increases.  $Ni_{50}Mn_{36}Sn_{14}$  Heusler alloy and its components undergo the hysteresis loops with soft magnetic characteristic, which has low coercivity, as the temperature approach to  $T_C$ . It is seen the remanence magnetizations ( $M_r$ ) of  $Ni_{50}Mn_{36}Sn_{14}$  HA and its components decrease as the temperature increases. As seen in Fig. 4b, its Mn

component displays a classic F hysteresis loop at  $T_1 < T < T_C$ . In that case, it can be suggested that its Mn2 component displays a weak first order phase transition at a temperature value between 1.00 to 1.25 according to the hysteresis behaviors. These ferromagnetic hysteresis behaviors are in a good accordance with the theoretical report of  $Ni_{50}Mn_{36}Sn_{14}$  Heusler alloy by Duran [35] and with the experimental reports of  $Ni_{50}Mn_{36}Sn_{14}$  alloy by Li et al. [66],  $Mn_2Ni_{1.6}Sn_{0.4}$  melt-spun ribbons by Singh et al. [67],  $Ni_{50}Mn_{36}Sn_{14-x}Si_x$  alloys by Raji et al. [29],  $Ni_{50}Mn_{40-x}Sn_{10+x}$  alloys by Aydogdu et al. [18].

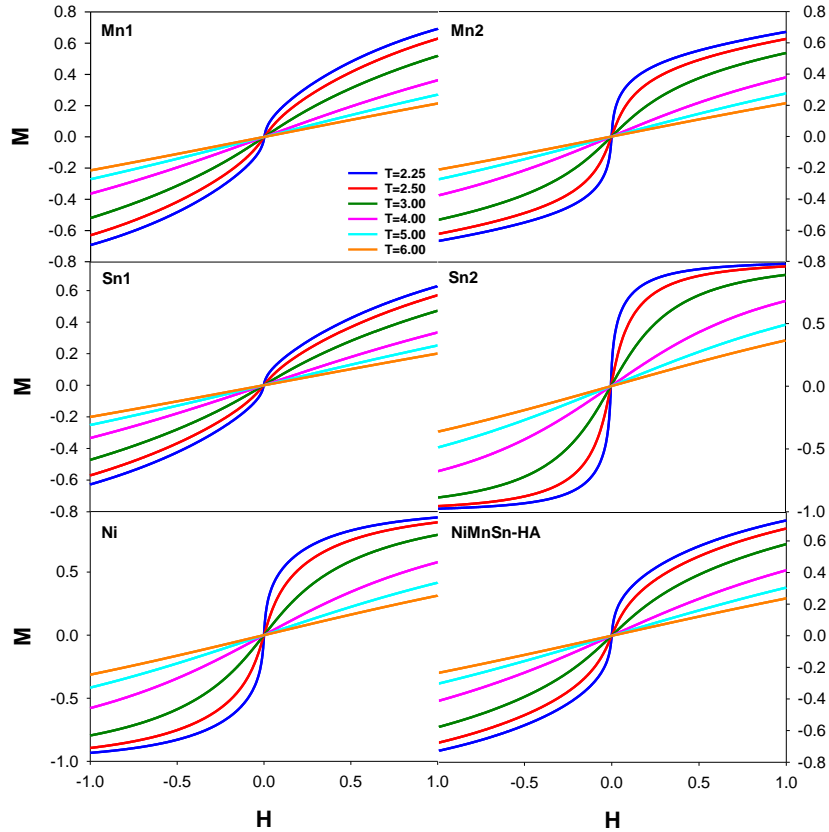


**Fig. 5.**  $M(H)$  magnetic hysteresis loops of (a) Mn1, (b) Mn2, (c) Sn1, (d) Sn2, (e) Ni component and (f) NiMnSn-HA for  $T > T_C$

The  $H_C$  values of the HA and its components are zero and the hysteresis loops of NiMnSn-HA and its components lose at  $T > T_C$  as it is seen in Fig. 5a-f. As the temperature increases, the hysteresis loops change into a straight line approaching the slope zero. Then, NiMnSn-HA and its components display P hysteresis behavior at  $T > T_C$ . This result is in agreement with P hysteresis behavior of NiMnSn-HA in our previous works [35, 36] and the  $Ni_{48}Co_2Mn_{39}Sn_{11}$  alloy by Cong et al. [68].

#### 4. CONCLUSIONS

The magnetic properties of  $Ni_{50}Mn_{36}Sn_{14}$  Heusler alloy with the antiferromagnetic exchange interaction between Mn2 and Sn1 components were investigated by using Kaneyoshi approach within the effective field theory.  $Ni_{50}Mn_{36}Sn_{14}$

Heusler alloy and its components display the second order phase transition from the ferromagnetic to the paramagnetic at  $T_C = 2.204$ . In addition, its Mn2 component also has the weak first order phase transition from ferromagnetic to ferromagnetic at  $T_1$ . On the other hand, it exhibits a reentrant phase transition. It can be said that its reentrant behavior is due to antiferromagnetic interaction between Mn2 and Sn1 components.  $Ni_{50}Mn_{36}Sn_{14}$  Heusler alloy and its components show a hard magnetic characteristic with high coercivity. Mn2 component exhibits a fluctuating ferromagnetic hysteresis behavior. And it can be said that the fluctuating ferromagnetic hysteresis behavior of Mn2 component is due to antiferromagnetic interaction between Mn2 and Sn1 components, below  $T_1$ . At  $T_1 < T < T_C$ , the hysteresis loops of NiMnSn-HA and its

components have the same coercive field ( $H_C$ ) decreasing as the temperature increases and they undergo soft magnetic characteristic, which has low coercivity, as the temperature approaches to  $T_C$ . NiMnSn-HA and its components have paramagnetic hysteresis curves at  $T > T_C$ . The numerical results in this work are in accordance with the some experimental and theoretical results of NiMnSn alloys. As a result, it can be suggested that its Mn<sub>2</sub> component displays a weak first order phase transition at a temperature value between 1.00 to 1.25 according to  $M(T)$  and  $M(H)$  curves. And it can be thought that NiMnSn-HA can be used in various applications as not only a soft ferromagnetic magnetic material due to its low coercivity near  $T_C$  and but also a hard ferromagnetic magnetic material due to its high coercivity at low temperature.

## 5. ACKNOWLEDGMENTS

This work was supported by Dumlupınar University Scientific Research Projects Commission (BAP: 2017-02).

## 6. REFERENCES

1. Kittel, C., 2005. Introduction to Solid State Physics (Eight Edition), John Wiley & Sons, New York, 352.
2. Wei, R., Sun, H., Chen, C., Tao, J., Li, F., 2018. Formation of Soft Magnetic High Entropy Amorphous Alloys Composites Containing *in Situ* Solid Solution Phase, J. Magn. Magn. Mater. 449, 63-67.
3. Becker, T.I., Zimmermann, K., Borin, D.Yu., Stepanov, G.V., Storozhenko, P.A. 2018. Dynamic Response of a Sensor Element Made of Magnetic Hybrid Elastomer with Controllable Properties. J. Magn. Magn. Mater. 449, 77-82.
4. Fan, L.F., Hsiang, H.I., Hung, J.J., 2018. Silane Surface Modification Effects on the Electromagnetic Properties of Phosphatized Iron-based SMCs. Applied Surface Science. 433, 133-138.
5. Alnasir, M. H., Awan, M.S., Manzoor, S., 2018. Magnetic and Magnetothermal Studies of Pure and Doped Gadolinium Silicide Nanoparticles for Self-controlled Hyperthermia Applications. J. Magn. Magn. Mater., 449, 137-144.
6. Hsiang, H.I., Fan, L.F., Hung, J.J., 2018. Phosphoric Acid Addition Effect on the Microstructure and Magnetic Properties of Iron-based Soft Magnetic Composites, J. Magn. Magn. Mater., 447, 1-8.
7. Jo Sunday, K., Taheri, M.L., 2017. Soft Magnetic Composites: Recent Advancements in the Technology, Metal Powder Report, 72(6) 425-429.
8. Lauda, M., Füzér, J., Kollár, P., Strečková, M., Bureš, R., Kováč, J., Bařková, M., Bařko, I., 2018. Magnetic Properties and Loss Separation in FeSi/MnZnFe<sub>2</sub>O<sub>4</sub> Soft Magnetic Composites, J. Magn. Magn. Mater., 411, 12-17.
9. Feng, S.J., Ni, J.L., Zhou, X.H., Wu, X.S., Huang, S.G., Liu, X.S., 2018. Expansion of Initial Magnetization Region in BaTi<sub>1.2</sub>Co<sub>1.2</sub>Fe<sub>9</sub>O<sub>19.8</sub> at Low Temperature. J. Magn. Magn. Mater., 447, 21-25.
10. Shen, J., Dai, Q., Ren, S., 2018. Phase Transformation Controlled Tetragonality of MnNi-based Nanocrystals, Nanotechnology, 27, 10LT01.
11. Fathi, R., Sanjabi, S., Bayat N., 2012. Synthesis and Characterization of NiMn Alloy Nanowires Via Electrodeposition in AAO Template, Materials Letters, 66, 346-348.
12. Li, C-M., Hu, Q-M., Yang, R., Johansson, B., Vitos, L., 2015. Theoretical Investigation of the Magnetic and Structural Transitions of Ni-Co-Mn-Sn Metamagnetic Shape-memory Alloys, Phys. Rev. B, 92, 024105.
13. Ignatiev, V.R., Lebedev, N.G., Orlov, A.A., 2018. Quantum Model of a Hysteresis in a Single-domain Magnetically Soft Ferromagnetic. J. Magn. Magn. Mater., 446, 135-142.
14. Conti S., Lenz, M. Rumpf, M. 2016. Hysteresis in Magnetic Shape Memory Composites: Modeling and Simulation, Journal of the Mechanics and Physics of Solids 89, 272-286.
15. Kantar, E., 2017. Composition, Temperature and Geometric Dependent Hysteresis Behaviours in Ising-type Segmented Nanowire

- with Magnetic and Diluted Magnetic, and its Soft/hard Magnetic Characteristics, *Philosophical Magazine*, 97(6), 431-450.
16. Popa, F., Chicinas, H.F., Marinca, T.F., Chicinas, I., 2017. Influence of Mechanical Alloying and Heat Treatment Processing on the Ni<sub>2</sub>MnSn Heusler Alloy Structure, *Journal of Alloys and Compounds*, 716, 137-143.
  17. Aydogdu, Y., Turabi, A.S., Aydogdu, A., Kok, M., Yakinci, Z.D., Karaca, H.E., 2016. The Effects of Boron Addition on the Magnetic and Mechanical Properties of NiMnSn Shape Memory Alloys, *Journal of Thermal Analysis and Calorimetry*, 126(2), 399-406.
  18. Aydogdu, Y., Turabi, A.S., Kok, M., Aydogdu, A., Yakinci, Z.D., Aksan, M.A., Yakinci, M.E., Karaca, H.E., 2016. The Effect of Sn Content on Mechanical, Magnetization and Shape Memory Behavior in NiMnSn, *J. Nanoalloys and Compounds*, 683, 339-345.
  19. Hernando, B., Sanchez Llamazares, J.L., Santos, J.D., Sanchez, M.L., Escoda, L., Sunol, J.J., Varga, N., Garcia, C., Gonzalez, J., 2009. Grain Oriented NiMnSn and NiMnIn Heusler Alloys Ribbons Produced by Melt Spinning: Martensitic Transformation and Magnetic Properties, *J. Magn. Magn. Mater.*, 321, 763-768.
  20. Lin, C., Yan, H., Zhang, Y., Esling, C., Zhao, X., Zuo, L., 2016. Crystal Structure of Modulated Martensite and Crystallographic Correlations Between Martensite Variants of Ni<sub>50</sub>Mn<sub>38</sub>Sn<sub>12</sub> Alloy, *Journal of Applied Crystallography* 49(4), 1276-1283.
  21. Chernenko, V.A., Barandiaran, J.M., L'vov, V.A., Gutierrez, J., Lazpita, P., Orue, I., 2013. Temperature Dependent Magnetostrains in Polycrystalline Magnetic Shape Memory Heusler Alloys, *Journal of Alloys and Compounds*, 577S, S305-S308.
  22. Guiza-Arguello, V.R., Monroe, J.A., Karaman, I., Hahn, M.S., 2010. Cytocompatibility Evaluation of NiMnSn Meta-magnetic Shape Memory Alloys for Biomedical Applications, *Journal of Biomedical Materials Research-Part B Applied Biomaterials*, 104(5), 853-863.
  23. Kainuma, R., Ito, K., Ito, W., Umetsu, R.Y., Kanomata, T., Ishida, K., 2010. NiMn-based Metamagnetic Shape Memory Alloys, *Materials Science Forum*, 635, 23-31.
  24. Wang, R.L., Yan, J.B., Marchenkov, V.V., Chen, S.S., Tang, S.L., Yang C.P., 2011. Effect of Al Doping on the Martensitic Transition and Magnetic Entropy Change in Ni-Mn-Sn Alloys, *Solid State Commun.*, 151, 1196-1199.
  25. de Groot, R.A., Van Engen, P.G., Van Engelen, P.P.T., Buschow, K.H.J., 1990. Magnetic and Magneto-optical Properties of NiMnSb<sub>1-x</sub>Sn<sub>x</sub> Compounds in Relation to Their Electronic Band Structure, *J. Magn. Magn. Mater.*, 86, 326-332.
  26. Huang, L., Cong, D.Y., Suo, H.L., Wang, Y.D., 2014. Giant Magnetic Refrigeration Capacity Near Room Temperature in Ni<sub>40</sub>Co<sub>10</sub>Mn<sub>40</sub>Sn<sub>10</sub> Multifunctional Alloy, *App. Phys. Lett.*, 104, 132407.
  27. Passamani, E.C., Cordova, C., Alves, A.L., Moscon, P.S., Larica, C., Takeuchi, A.Y., Biondo, A., 2009. Magnetic studies of Fe-Doped Martensitic Ni<sub>2</sub>Mn<sub>1.44</sub>Sn<sub>0.56</sub> Heusler alloy, *J. Phys. D: Appl. Phys.*, 42, 215006.
  28. Llamazares, J.L.S., Zuniga, H.F., Jara, D.R., Valdes, C.F.S., Fernandez, T.G., Ross, C.A., Garcia, C., 2013. Structural and Magnetic Characterization of the Intermartensitic Phase Transition in NiMnSn Heusler Alloy Ribbons, *J. App. Phys.*, 113, 17A948.
  29. Raji, G.R., Uthaman, B., Rajan, R.K., Sharannia, M.P., Thomas, S., Suresh, K.G., Varma M.R., 2016. Martensitic Transition, Spin Glass Behavior and Exchange Bias in Si Substituted Ni<sub>50</sub>Mn<sub>36</sub>Sn<sub>14</sub> Heusler Alloys, *RSC Advances*, 6, 32037-32045.
  30. Grünebohm, A., Herper, H.C., Entel, P., 2016. On the Rich Magnetic Phase Diagram of (Ni, Co)-Mn-Sn Heusler Alloys, *Journal of Physics D: Applied Physics*, 49(39), 395001.
  31. Wang, X., Shang, J., Wang, F., Jiang, C., Xu, H., 2014. Origin of Unusual Properties in the Ferromagnetic Heusler Alloy Ni-Mn-Sn: A First-principles Investigation, *Scripta Materialia*, 89, 33-36.
  32. Siewert, M., Gruner, M.E., Hucht, A., Herper, H.C., Dannenberg, A., Chakrabarti, A., Singh, N., Arroyave, R., Entel, P., 2012. A First-Principles Investigation of the Compositional Dependent Properties of Magnetic Shape

- Memory Heusler Alloys, *Advanced Engineering Mater.*, 63, 1-17.
33. Xiao, H.B., Yang, C.P., Wang, R.L., Marchenkov, V.V., Luo, X., 2014. Martensitic Transformation and Phase Stability of In-doped Ni-Mn-Sn Shape Memory Alloys from First-Principles Calculations, *J. App. Phys.*, 115, 203703.
34. Grünebohm, A., Comtesse, D., Hucht, A., Gruner, M.E., Maslovskaya, A., Entel, P., 2014. Optimizing the Magnetocaloric Effect in Ni-Mn-Sn by Substitution: a First-principles Study, *IEEE Transactions on Magnetics*, 50 (11), 2506004.
35. Duran, A., 2018. Lattice Location Effect of Ni<sub>50</sub>Mn<sub>36</sub>Sn<sub>14</sub> Heusler Alloy, *J. Supercond Nov Magn.*, 31 (4), 1101-1109.
36. Duran, A., 2018. Lattice Location Effect of Ni<sub>50</sub>Mn<sub>36</sub>Sn<sub>14</sub> Heusler Alloy, *J. Supercond Nov Magn.*, doi: 10.1007/s10948-018-4686-8 (first online)
37. Kaneyoshi, T., 2009. Magnetizations of a Nanoparticle Described by the Transverse Ising Model, *J. Magn. Magn. Mater.*, 321, 3430-3435.
38. Kaneyoshi, T., 2010. Phase Diagrams of a Transverse Ising Nanowire, *J. Magn. Magn. Mater.*, 322, 3014-3018.
39. Kaneyoshi, T., 2012. The Possibility of a Compensation Point Induced by a Transverse Field in Transverse Ising Nanoparticles With a Negative Core-shell Coupling, *Solid State Commun.*, 152, 883-886.
40. Kaneyoshi, T., 2009. Ferrimagnetic Magnetizations of Transverse Ising Thin Films With Diluted Surfaces, *J. Magn. Magn. Mater.*, 321, 3630-3636.
41. Keskin, M., Şarlı, N., 2017. Magnetic Properties of the Binary Nickel/Bismuth Alloy, *J. Magn. Magn. Mater.*, 437, 1-6.
42. Wang, C.D., Ma, R.G., 2013. Force Induced Phase Transition of Honeycomb-structured Ferroelectric Thin Film, *Physica A*, 392, 3570-3577.
43. Şarlı, N., 2016. Generation of an External Magnetic Field With the Spin Orientation Effect in a Single Layer Ising Nanographene, *Physica E*, 83, 22-29.
44. Şarlı, N., Akbudak, S., Ellialtıođlu, M.R., 2014. The Peak Effect (PE) Region of the Antiferromagnetic Two Layer Ising Nanographene, *Physica B*, 452, 18-22.
45. Şarlı, N., Akbudak, S., Polat, Y., Ellialtıođlu, M.R., 2015. Effective Distance of a Ferromagnetic Trilayer Ising Nanostructure With an ABA Stacking Sequence, *Physica A*, 434, 194-200.
46. Şarlı, N., 2016. Artificial Magnetism in a Carbon Diamond Nanolattice With the Spin Orientation Effect, *Diamond & Related Materials*, 64, 103-109.
47. Kantar, E., Keskin, M., 2014. Thermal and Magnetic Properties of Ternary Mixed Ising Nanoparticles With Core-shell Structure: Effective-field Theory Approach, *J. Magn. Magn. Mater.*, 349, 165-172.
48. Jiang, W., Li, X.-X., Liu, L.-M., Chen, J.-N., Zhang, F., 2014. Hysteresis Loop of a Cubic Nanowire in the Presence of the Crystal Field and the Transverse Field. *J. Magn. Magn. Mater.* 353, 90-98.
49. Şarlı, N., 2015. Paramagnetic Atom Number and Paramagnetic Critical Pressure of the sc, bcc and fcc Nanolattices, *J. Magn. Magn. Mater.*, 374, 238-244.
50. Ertaş, M., Kocakaplan, Y., 2014. Dynamic Behaviors of the Hexagonal Ising Nanowire, *Phys. Lett. A*, 378, 845-850.
51. Zaim, A., Kerouad, M., Boughrara, M., 2013. Effects of the Random Field on the Magnetic Behavior of Nanowires With Core/shell Morphology, *J. Magn. Magn. Mater.*, 331, 37-44.
52. Bouhou, S., Essaoudi, I., Ainane, A., Saber, M., Ahuja, R., Dujardin, F., 2013. Phase Diagrams of Diluted Transverse Ising Nanowire, *J. Magn. Magn. Mater.*, 336, 75-82.
53. Jiang, W., Li, X.X., Liu, L.M., 2013. Surface Effects on a Multilayer and Multisublattice Cubic Nanowire With Core/shell, *Physica E*, 53, 29-35.
54. Akıncı, Ü., 2012. Effects of the Randomly Distributed Magnetic Field on the Phase Diagrams of Ising Nanowire I: Discrete Distributions, *J. Magn. Magn. Mater.*, 324(22), 3951-3960.

55. Keskin, M., Şarlı, N., Deviren, B., 2011. Hysteresis Behaviors in a Cylindrical Ising Nanowire, *Solid State Commun.*, 151, 1025-1030.
56. Şarlı, N., Keskin, M., 2012. Two Distinct Magnetic Susceptibility Peaks and Magnetic Reversal Events in a Cylindrical Core/shell Spin-1 Ising Nanowire, *Solid State Commun.*, 152, 354-359.
57. Magoussi, H., Zaim, A., Kerouad, M., 2013. Effects of the Trimodal Random Field on the Magnetic Properties of a Spin-1 Nanotube, *Chin. Phys. B*, 22(11), 116401.
58. Deviren, B., Şener, Y., Keskin, M., 2013. Dynamic Magnetic Properties of the Kinetic Cylindrical Ising Nanotube, *Physica A*, 392, 3969-3983.
59. Kocakaplan, Y., Kantar, E., Keskin, M., 2013. Hysteresis Loops and Compensation Behavior of Cylindrical Transverse Spin-1 Ising Nanowire with the Crystal Field Within Effective-field Theory Based on a Probability Distribution Technique, *The European Physical Journal B*, 86, 420.
60. Şarlı, N., 2015. Superconductor Core Effect of the Body Centered Orthorhombic Nanolattice Structure, *J. Supercond Nov Magn.*, 28(8), A014, 2355-2363.
61. Şarlı, N., 2014. The Effects of Next Nearest-neighbor Exchange Interaction on the Magnetic Properties in the One-dimensional Ising System, *Physica E: Low-Dimensional Systems and Nanostructures*, 63, 324-328.
62. Kantar, E., 2017. Superconductivity-like Phenomena in an Ferrimagnetic Endohedral Fullerene with Diluted Magnetic Surface, *Solid State Commun.*, 263, 31-37.
63. Özkan, A., Kutlu, B., 2016. The Effect of the Heating Rate on the Phase Transition, *Phase Transitions*, 89 (12) 1183-1195.
64. Binder, K., 1987. Theory of First-order Phase Transitions, *Rep Prog Phys.*, 50, 783-859.
65. Fernandes, LA, Ruiz-Lorenzo, J.J, Lombardo, M.P., Tarancon, A., 1992. Weak First Order Transitions. The Two-dimensional Potts Model, *Phys. Lett. B.*, 277, 485-490.
66. Li, Z., Jing, C., Chen, J., Yuan, S., Cao, S., Zhang, J., 2007. Observation of Exchange Bias in the Martensitic State of  $\text{Ni}_{50}\text{Mn}_{36}\text{Sn}_{14}$  Heusler Alloy, *Appl. Phys. Lett.*, 91, 112505.
67. Singh, N., Borgahain, B., Srivastava, A.K., Dhar, A., Singh, H.K., 2016. Magnetic Nature of Austenite-martensite Phase Transition and Spin Glass Behaviour in Nanostructured  $\text{Mn}_2\text{Ni}_{1.6}\text{Sn}_{0.4}$  Melt-spun Ribbons, *Appl. Phys. A*, 122 (3), 237.
68. Cong, D.Y., Roth, S., Wang, Y. D., 2014. Superparamagnetism and Superspin Glass Behaviors in Multiferroic NiMn-based Magnetic Shape Memory Alloys, *Phys. Status Solidi (B)*, 251(10), 2126-2134.

